

Fast optimal CMB power spectrum estimation with Hamiltonian sampling

J. F. Taylor ^{*}, M. A. J. Ashdown and M. P. Hobson

Astrophysics Group, Cavendish Laboratory, JJ Thomson Avenue, Cambridge CB3 0HE, UK

Accepted —. Received —; in original form 24 October 2018

ABSTRACT

We present a method for fast optimal estimation of the temperature angular power spectrum from observations of the cosmic microwave background. We employ a Hamiltonian Monte Carlo (HMC) sampler to obtain samples from the posterior probability distribution of all the power spectrum coefficients given a set of observations. We compare the properties of the HMC and the related Gibbs sampling approach on low-resolution simulations and find that the HMC method performs favourably even in the regime of relatively low signal-to-noise. We also demonstrate the method on high-resolution data by applying it to simulated *WMAP* data. Analysis of a *WMAP*-sized data set is possible in a around eighty hours on a high-end desktop computer. HMC imposes few conditions on the distribution to be sampled and provides us with an extremely flexible approach upon which to build.

Key words: cosmic microwave background – methods: data analysis – methods: statistical

1 INTRODUCTION

Observations of the cosmic microwave background (CMB) have proved to be extremely valuable for testing and constraining cosmological models. The majority of models predict that the anisotropies in the CMB signal are Gaussian and their statistics isotropic across the sky. The angular power spectrum C_ℓ therefore provides a natural connection between theory and observation and a variety of methods have been explored to compute the power spectrum from sets of observations.

Maximum-likelihood methods (Gorski 1994; Bond, Jaffe & Knox 1998; Oh, Spergel & Hinshaw 1999) provide an optimal estimate of the CMB power spectrum which has made them an invaluable tool for analysing the CMB for single-dish experiments and interferometers (Hobson & Masinger 2002). Brute force implementations of the method can only be applied to small data sets as the required computation scales as $\mathcal{O}(N_{\text{pix}}^3)$, where N_{pix} is the number of pixels in a CMB map (see Efstathiou (2003) for a review). For a number of special cases one can construct maximum-likelihood estimators that perform more favourably (Challinor et al. 2002; Wandelt & Hansen 2003), although their lack of generality limits their applicability and, as their computational demands scale as $\mathcal{O}(N_{\text{pix}}^2)$, even they cannot be applied directly the largest contemporary (*WMAP*) or future (*Planck*) data.

Alternatively one can resort to approximate pseudo- C_ℓ methods, Hivon et al. (2002). These scale as the map-making process and are fast even for the largest data sets. Hybrid methods (Efstathiou 2004) combine a maximum-likelihood approach

on large angular scales with a fast pseudo- C_ℓ estimator on small scales.

To compare theoretically predicted power spectra and those estimated from a set of observations it is necessary to construct a likelihood function. Maximum-likelihood and pseudo- C_ℓ methods can only provide approximations to this likelihood.

An alternative framework has been developed (Wandelt, Larson & Laksminarayana 2004; Jewell, Levin & Anderson 2004) where one explores the full posterior distribution of the power spectrum with Monte Carlo samples. This method is not only exact but scales like the pseudo- C_ℓ methods. Under the assumption of position invariant, circularly symmetric beams and uncorrelated noise, one can perform the beam convolution in the spherical harmonic domain and evaluate the likelihood of the data in the map domain, and the method scales as $\mathcal{O}(N_{\text{pix}}^{3/2})$. The favourable scaling has enabled the method to be applied to the *WMAP* data (Bennett et al. 2003; Eriksen et al. 2004).

The approach relies on the availability of an efficient method for sampling from high-dimensional distributions. Previous implementations use a Gibbs sampler but this restricts the applicability of the method to Gaussian noise and CMB. We propose the use of a Hamiltonian Monte Carlo (HMC) sampler (Duane et al. 1987). As opposed to the majority of Markov-Chain Monte Carlo (MCMC) methods, HMC scales well with problem size. Few requirements are made on the distribution to be sampled, thus giving us the opportunity for great flexibility. HMC has been widely applied in Bayesian computation (Neal 1993) and has also been employed for cosmological parameter estimation (Hajian 2007).

In this work we begin, in Section 2, by outlining the procedure for estimating power spectra with sampling. In Section 3 we

* E-mail: j.taylor@mrao.cam.ac.uk

2 Taylor, Ashdown & Hobson

describe the HMC method and a technique for determining the convergence of samples drawn with a HMC sampler. A summary of the process of applying HMC to the power spectrum estimation problem can be found in Section 4 and we provide a prescription for setting the many tuneable parameters of the sampler. In Section 5 we apply the method to low-resolution simulations and compare the Hamiltonian and Gibbs samplers. Section 6 details our application of the method to simulated *WMAP* observations. Our conclusions are presented in Section 7.

2 POWER SPECTRUM ESTIMATION WITH SAMPLING

Suppose the true CMB sky, divided for convenience into pixels, is represented by the temperature vector \mathbf{t} . The sky is observed and the resultant data vector \mathbf{d} , in any domain, is the sum $\mathbf{d} = \mathbf{s} + \mathbf{n}$ of contributions due to the underlying CMB signal \mathbf{s} in that domain and the corresponding noise \mathbf{n} . Moreover the signal \mathbf{s} is usually linearly related to the true CMB sky \mathbf{t} . Thus we have

$$\mathbf{d} = \mathbf{R}\mathbf{t} + \mathbf{n}, \quad (1)$$

where the matrix \mathbf{R} represents the linear mapping from the true CMB sky to the corresponding CMB signal in whatever domain the data resides.

In the following discussion, we need not assume a particular domain for the generic data vector \mathbf{d} . Nevertheless, it is most common for \mathbf{d} to represent the pixelised CMB map convolved with the instrument beam and our work, so far, has used solely this form for the data vector.

The temperature field \mathbf{t} is related to the spherical harmonic coefficients of the field \mathbf{a} by

$$t(x_p) = \sum_{\ell=2}^{\ell_{\max}} \sum_{m=-\ell}^{\ell} a_{\ell m} Y_{\ell m}(x_p), \quad (2)$$

where $t(x_p)$ is a single pixel in the map vector \mathbf{t} and the $Y_{\ell m}$ are the spherical harmonics. Although formally one may take the upper limit of the ℓ summation to be infinite, it is more typical to choose a finite value for ℓ_{\max} appropriate to the beam size. We have not considered the effect of the mono- and dipole contributions, the handling of which, within this framework, is discussed in Eriksen et al. (2004). In this notation we may write our model for the data in the form

$$\mathbf{d} = \mathbf{R}\mathbf{Y}\mathbf{a} + \mathbf{n}, \quad (3)$$

where \mathbf{Y} describes the application of the spherical harmonic transform and we represent the spherical harmonic coefficients by a real vector.

For an isotropic Gaussian CMB sky the covariance matrix \mathbf{C} of the $a_{\ell m}$ has components

$$C_{\ell m \ell' m'} = \langle a_{\ell m} a_{\ell' m'}^* \rangle = C_{\ell} \delta_{\ell \ell'} \delta_{m m'}, \quad (4)$$

where the set of coefficients $\{C_{\ell}\}$ constitute the theoretical angular power spectrum. Note that, since the sky is real, $a_{\ell m} = a_{\ell, -m}^*$.

We aim to sample from the joint distribution of the power spectrum coefficients $\Pr(\{C_{\ell}\}|\mathbf{d})$. Although this is difficult to perform directly, it is possible to sample from the joint density of the power spectrum coefficients and the signal realization $\Pr(\{C_{\ell}\}, \mathbf{a}|\mathbf{d})$ and then marginalise over \mathbf{a} . The joint density can be written as the product of the appropriate conditional distributions

$$\Pr(\{C_{\ell}\}, \mathbf{a}|\mathbf{d}) \propto \Pr(\mathbf{d}|\mathbf{a}) \Pr(\mathbf{a}|\{C_{\ell}\}) \Pr(\{C_{\ell}\}). \quad (5)$$

The choice of prior $\Pr(\{C_{\ell}\})$ is an interesting topic. Wandelt et al. (2004) have some suggestions for making this choice but for the purpose of this work we set $\Pr(\{C_{\ell}\}) = 1$ so that the maximum of our posterior will correspond directly to a maximum-likelihood estimate.

Given our choice of prior and assuming the noise is Gaussian then the conditional distributions that make up (5) can be written in the form

$$\Pr(\mathbf{d}|\mathbf{a}) \propto \exp\left[-\frac{1}{2}(\mathbf{d} - \mathbf{R}\mathbf{Y}\mathbf{a})^T \mathbf{N}^{-1}(\mathbf{d} - \mathbf{R}\mathbf{Y}\mathbf{a})\right], \quad (6)$$

where $\mathbf{N} = \langle \mathbf{n}\mathbf{n}^T \rangle$, and

$$\Pr(\mathbf{a}|\{C_{\ell}\}) \propto \frac{1}{\sqrt{|\mathbf{C}|}} \exp\left(-\frac{1}{2}\mathbf{a}^T \mathbf{C}^{-1} \mathbf{a}\right) \quad (7)$$

where \mathbf{C} is easily constructed using (4). It is convenient to rewrite this in the form

$$\Pr(\mathbf{a}|\{C_{\ell}\}) \propto \prod_{\ell=2}^{\ell_{\max}} \left(\frac{1}{C_{\ell}}\right)^{\frac{2\ell+1}{2}} \exp\left(-\frac{2\ell+1}{2} \frac{\sigma_{\ell}}{C_{\ell}}\right), \quad (8)$$

where $\sigma_{\ell} = \frac{1}{2\ell+1} \sum_m |a_{\ell m}|^2$ is the power spectrum of the signal realization.

The selection of a domain in which to represent the data is determined by the requirement that \mathbf{N} has a simple form. In this work we make the assumption that in the map domain \mathbf{N} is well represented by a diagonal matrix. In this domain incomplete sky coverage is straightforwardly handled by setting the elements of \mathbf{N}^{-1} that correspond to excluded pixels to zero. If the instrument beam is position invariant and circularly symmetric then we can compute the beam convolution quickly in harmonic space and the predicted noiseless data can be written in the form $\mathbf{Y}\mathbf{B}\mathbf{a}$ where \mathbf{B} represents the smoothing by the beam.

The computational cost of evaluating the posterior (and its gradients) is now limited by the speed at which one can compute the spherical harmonic transform \mathbf{Y} . The transforms scale as $\mathcal{O}(N_{\text{pix}}^{3/2})$ and can be efficiently parallelised.

We draw samples from the joint space $(\mathbf{a}, \{C_{\ell}\})$ using a Hamiltonian Monte-Carlo sampler described in Section 3.

3 HAMILTONIAN MONTE CARLO

Let us suppose that we wish to draw samples from a target density $\Pr(\mathbf{x})$, where \mathbf{x} is the N -dimensional vector of our parameters. Conventional MCMC methods move through the parameter space by a random walk and therefore require a prohibitive number of samples to explore high dimensional spaces. The Hamiltonian Monte Carlo method (Duane et al. 1987; Neal 1993, 1996) draws parallels between sampling and classical dynamics. By exploiting techniques developed for describing the motion of particles in potentials it is possible to suppress random walk behaviour. Introducing persistent motion of the chain through the parameter space allows HMC to maintain a reasonable efficiency even for high dimensional problems (Hanson 2001).

For each parameter, x_i we introduce a ‘momentum’ p_i and a ‘mass’ m_i ; we discuss how to set the mass in the Appendix. We construct a Hamiltonian formed from a potential energy term $\psi(\mathbf{x})$ and a kinetic energy term such that

$$H = \sum_i \frac{p_i^2}{2m_i} + \psi(\mathbf{x}), \quad (9)$$

where our potential is related to the target density by

$$\psi(\mathbf{x}) = -\log \Pr(\mathbf{x}). \quad (10)$$

Our new objective is to draw samples from a distribution that is proportional to $\exp(-H)$. The form of the Hamiltonian is such that this distribution is separable into a Gaussian in \mathbf{p} and the target distribution, i.e.

$$\exp(-H) = \Pr(\mathbf{x}) \prod_i \exp\left(-\frac{p_i^2}{2m_i}\right). \quad (11)$$

We can then obtain samples from $\Pr(\mathbf{x})$ by marginalising over \mathbf{p} .

To find a new sample we first draw a set of momenta from the distribution defined by our kinetic energy term, i.e. an N dimensional uncorrelated Gaussian with a variance in dimension i of m_i . We then allow our system to evolve deterministically, from our starting point (\mathbf{x}, \mathbf{p}) in the phase space for some fixed time τ according to Hamilton's equations,

$$\frac{dx_i}{dt} = \frac{\partial H}{\partial p_i} \quad (12)$$

$$\frac{dp_i}{dt} = -\frac{\partial H}{\partial x_i} = -\frac{\partial \psi(\mathbf{x})}{\partial x_i}. \quad (13)$$

At the end of this trajectory we have reached the point $(\mathbf{x}', \mathbf{p}')$ and we accept this point with probability

$$p_A = \min(1, \exp(-\delta H)), \quad (14)$$

where

$$\delta H = H(\mathbf{x}', \mathbf{p}') - H(\mathbf{x}, \mathbf{p}). \quad (15)$$

After a new proposed sample is generated the momentum variable is discarded and the process restarts by randomly drawing a new set of momenta as described above.

This implies that if we are able to integrate Hamilton's equations exactly then, as energy is conserved along such a trajectory, the probability of acceptance is unity.

In fact the method is more general as, provided one uses the Metropolis acceptance criterion (14), it is permitted to follow any trajectory to generate a new candidate point. However only trajectories that approximately conserve the value of the Hamiltonian (9) will result in high acceptance rates. For some problems it may be advantageous to generate trajectories using an approximate Hamiltonian that can be computed rapidly, and bear the cost of lowering the acceptance probability.

To integrate the equations of motions it is common practice to use the leapfrog method. This method has the property of exact reversibility which is required to ensure the chain satisfies detailed balance. It is also numerically robust and allows for the simple propagation of errors. We make n steps with a finite step size ϵ , such that $n\epsilon = \tau$, as follows,

$$p_i\left(t + \frac{\epsilon}{2}\right) = p_i(t) - \frac{\epsilon}{2} \frac{\partial \psi(\mathbf{x})}{\partial x_i} \Bigg|_{\mathbf{x}(t)} \quad (16)$$

$$x_i(t + \epsilon) = x_i(t) + \frac{\epsilon}{m_i} p_i\left(t + \frac{\epsilon}{2}\right) \quad (17)$$

$$p_i(t + \epsilon) = p_i\left(t + \frac{\epsilon}{2}\right) - \frac{\epsilon}{2} \frac{\partial \psi(\mathbf{x})}{\partial x_i} \Bigg|_{\mathbf{x}(t+\epsilon)} \quad (18)$$

until $t = \tau$. The interval τ must be varied, usually by drawing n and ϵ randomly from uniform distributions, to avoid resonant trajectories. Higher-order integration schemes are permitted, provided exact reversibility is maintained, although generally incur significant additional computational costs.

3.1 Convergence tests

Diagnosing the convergence of a chain in an MCMC process is the subject of much literature (see Cowles & Carlin (1996); Brooks & Roberts (1997) for comprehensive reviews). Hanson (2001) provides a method that uses the gradient information, which we must possess to calculate trajectories in HMC, to compute a convergence criteria.

One constructs two estimates of the variance of a chain, that depend quite differently upon the distribution of samples across the target density, although the basic method is easily generalised to (combinations of) higher order central moments of $\Pr(\mathbf{x})$. When the two estimates agree to within a certain accuracy the chain is assumed to have converged.

We compute the variance of each parameter x_i independently. Our first estimate of the variance of the samples is calculated by

$$\sigma_i^2 = \int (x_i - \bar{x}_i)^2 \Pr(\mathbf{x}) d\mathbf{x} \approx \frac{1}{M} \sum_k (x_i^k - \bar{x}_i)^2, \quad (19)$$

where k labels a sample in a chain of M samples and the integral extends over the entire \mathbf{x} -space. For our second estimate we take the expression for the variance and integrate by parts

$$\begin{aligned} \sigma_i^2 &= \int (x_i - \bar{x}_i)^2 \Pr(\mathbf{x}) d\mathbf{x} \\ &= \frac{1}{3} \left| (x_i - \bar{x}_i)^3 \Pr(x_i) \right|_{-\infty}^{\infty} \\ &\quad - \frac{1}{3} \int (x_i - \bar{x}_i)^3 \frac{\partial \Pr(\mathbf{x})}{\partial x_i} d\mathbf{x}, \end{aligned} \quad (20)$$

the first term of which will vanish if the marginalized distribution $\Pr(x_i)$ drops off faster than x_i^3 as x_i tends to $\pm\infty$. Using (10) we rewrite this expression as

$$\sigma_i^2 = \frac{1}{3} \int_{-\infty}^{\infty} (x_i - \bar{x}_i)^3 \frac{\partial \psi(\mathbf{x})}{\partial x_i} \Pr(\mathbf{x}) d\mathbf{x}. \quad (21)$$

We compute (21) from the samples in our chain by

$$\sigma_i^2 \approx \frac{1}{M} \frac{1}{3} \sum_k (x_i^k - \bar{x}_i)^3 \frac{\partial \psi}{\partial x_i} \Bigg|_{x_i^k}. \quad (22)$$

To test for convergence we compute the ratio R_i of (19) and (22), and we believe the chain has converged when all the R_i are close to unity.

We have tested how this criterion compares to the widely used Gelman-Rubin statistic (Gelman & Rubin 1992) and have found that Hanson's method tends to be, if anything, slightly pessimistic. We find that values of R in the range 0.8 to 1.2 represent good convergence and values in the range 0.6 to 1.4 are acceptable. The Gelman-Rubin method requires multiple chains to be generated and compares inter-chain with intra-chain statistics, whereas Hanson's test uses a single chain and compares two different intra-chain statistics. We use the Hanson test as it is very easy to compute, scales well with problem size and requires that we only generate one chain. We plan to explore other intra-chain convergence diagnostics such as that proposed by Dunkley et al. (2005).

4 HAMILTONIAN MONTE CARLO AND POWER SPECTRUM ESTIMATION

We use HMC to draw samples simultaneously from the joint density (5). Our potential is defined by $\psi(\mathbf{a}, \{C_\ell\}) =$

4 Taylor, Ashdown & Hobson

– log Pr ($\mathbf{a}, \{C_\ell\} | \mathbf{d}$) such that

$$\begin{aligned} \psi(\mathbf{a}, \{C_\ell\}) &= \frac{1}{2} (\mathbf{d} - \mathbf{YB}\mathbf{a})^T \mathbf{N}^{-1} (\mathbf{d} - \mathbf{YB}\mathbf{a}) \\ &+ \sum_\ell \left(\ell + \frac{1}{2} \right) \left(\ln C_\ell + \frac{\sigma_\ell}{C_\ell} \right) + \text{const} \end{aligned} \quad (23)$$

and the gradient of the potential can be computed exactly by

$$\frac{\partial \psi(\mathbf{a}, \{C_\ell\})}{\partial \mathbf{a}} = -\mathbf{B}\mathbf{Y}^T \mathbf{N}^{-1} (\mathbf{d} - \mathbf{YB}\mathbf{a}) + \mathbf{C}^{-1} \mathbf{a} \quad (24)$$

$$\frac{\partial \psi(\mathbf{a}, \{C_\ell\})}{\partial C_\ell} = \left(\ell + \frac{1}{2} \right) \frac{1}{C_\ell} \left(1 - \frac{\sigma_\ell}{C_\ell} \right). \quad (25)$$

The positivity requirement on the power spectrum C_ℓ can result in a high rejection rate and we have found it advantageous to reparametrize the problem in terms of the logarithm of the C_ℓ s. For this reparametrization it is easy to calculate the corresponding potential and its derivatives. To enforce a flat prior on each C_ℓ we must apply an exponential prior on log C_ℓ .

To generate a new sample requires us to evaluate the gradient at each point along the leapfrog trajectory and to evaluate the value of the potential once at the end of the trajectory. Therefore, if we take n leapfrog steps, we must perform $2n + 1$ spherical harmonic transforms, although we can reuse the gradient at the end of one trajectory for the first step of the next.

We split the sampling process into a burn in phase, in which we attempt to lose any dependence on our starting point, and a sampling phase where we store the samples from the chain and we believe these samples are drawn from the target density. During burn in we are permitted to adjust the parameters of the sampler, for example to tune the acceptance rate. Once burn in is complete we must fix the parameters of the sampler in order that our samples come from the desired distribution.

A good starting point can significantly reduce the time required for burn in. We have explored a number of possibilities for computing a starting point for the signal \mathbf{a} given some initial guess for the power spectrum. One we have found particularly effective is to draw a single signal sample, as for one step of the Gibbs sampler, from the conditional distribution Pr ($\mathbf{a} | \mathbf{d}, \{C_\ell\}$). This is a computationally expensive process and is described fully in Wandelt et al. (2004); Eriksen et al. (2004). The basic procedure involves solving the following equation for \mathbf{x} , the spherical harmonic coefficients of the mean field (Wiener filtered) map,

$$(\mathbf{C}^{-1} + \mathbf{B}\mathbf{Y}^T \mathbf{N}^{-1} \mathbf{YB}) \mathbf{x} = \mathbf{B}\mathbf{Y}^T \mathbf{N}^{-1} \mathbf{d} \quad (26)$$

and a fluctuation term \mathbf{y} that corrects for the bias in \mathbf{x}

$$(\mathbf{C}^{-1} + \mathbf{B}\mathbf{Y}^T \mathbf{N}^{-1} \mathbf{YB}) \mathbf{y} = \mathbf{C}^{-1/2} \omega_0 + \mathbf{B}\mathbf{Y}^T \mathbf{N}^{-1/2} \omega_1, \quad (27)$$

where ω_0 is a set of spherical harmonic coefficients and ω_1 a map both containing Gaussian white noise of zero mean and unit variance. The sum of \mathbf{x} and \mathbf{y} is our starting sample \mathbf{a} . We solve for $\mathbf{x} + \mathbf{y}$ using a conjugate gradient algorithm (see, for example Golub & Loan (1996)). A preconditioner can be used to reduce the number of iterations required for the convergence of the conjugate gradient solver, however the construction of a preconditioner is itself a complex procedure, and since we only perform this step once and the accuracy of the result is of little consequence, we have not made use of one in this work. Whether or not applying the conjugate gradient algorithm without a preconditioner is feasible depends on the nature of the data set under consideration.

HMC has a large number of adjustable parameters, notably the masses. The distribution for the \mathbf{a} parameters is Gaussian and so we attempt to set the mass associated with each $a_{\ell m}$ such that they are

inversely proportional to the variance of that $a_{\ell m}$. We justify this choice in the Appendix. The masses for the \mathbf{a} are estimated for a fixed power spectrum for which the variance is computed by

$$\text{var}(a_{\ell m}) = (C_\ell^{-1} + B_\ell N_{\ell m, \ell' m'}^{-1} \delta_{\ell \ell'} \delta_{m m'} B_\ell)^{-1}, \quad (28)$$

where we use our initial estimate of the power spectrum as the value of C_ℓ and compute the diagonal elements of the inverse noise covariance matrix in harmonic space using Monte Carlo simulations.

At high ℓ and with good signal-to-noise the marginal distributions for each C_ℓ are close to Gaussian and we can obtain masses from the standard expression for the variance (see, for example Zaldarriaga & Seljak (1997))

$$\text{var}(C_\ell) = \frac{2\ell + 1}{2f_{\text{sky}}} (C_\ell + N_\ell/B_\ell^2)^2, \quad (29)$$

where N_ℓ is the power spectrum of the noise in the data, B_ℓ is the beam transfer function and f_{sky} is the fraction of the sky observed. For low multipoles the distributions are significantly skewed and in low signal-to-noise the sharp cut off of the distribution at $C_\ell = 0$ has a similar effect. In these cases we have found that setting the masses from the variances is insufficient. Instead we tune these masses empirically. We aim to set the mass for each parameter to as small a value as possible while maintaining our target acceptance rate. We sample the C_ℓ s from simple approximate likelihood function and gradually reduce the masses until the acceptance rate drops. This gives masses that are sufficient for sampling the full problem efficiently.

During burn in we can further tune the masses; the convergence criterion for each parameter providing a good indication of whether or not the mass associated with that parameter is set correctly.

We must randomise the length of each trajectory and have found that drawing n from a uniform distribution between 10 and 20 is appropriate. Therefore we typically require the application of ~ 30 spherical harmonic transforms to generate a new proposed sample. We then tune the step size ϵ such that we obtain an acceptance rate between 70 and 90 per cent. A higher acceptance rate is used for HMC than other MCMC methods as the computational cost of a rejection is so high.

Once sampling we store each $\{C_\ell\}$ sample and the realization power spectrum $\{\sigma_\ell\}$ of each signal sample. The $\{\sigma_\ell\}$ can be used to form the Blackwell-Rao estimator of the posterior distribution (Chu et al. 2005). The posterior can be written

$$\begin{aligned} \text{Pr}(\{C_\ell\} | \mathbf{d}) &= \int \text{Pr}(\{C_\ell\}, \mathbf{a} | \mathbf{d}) \, d\mathbf{a} \\ &= \int \text{Pr}(\{C_\ell\} | \mathbf{a}) \text{Pr}(\mathbf{a} | \mathbf{d}) \, d\mathbf{a}, \end{aligned} \quad (30)$$

which for a Gaussian CMB can be written as

$$\text{Pr}(\{C_\ell\} | \mathbf{d}) = \int \text{Pr}(\{C_\ell\} | \{\sigma_\ell\}) \text{Pr}(\{\sigma_\ell\} | \mathbf{d}) \, d\{\sigma_\ell\}, \quad (31)$$

where

$$\text{Pr}(\{C_\ell\} | \{\sigma_\ell\}) = \prod_\ell \frac{1}{\sigma_\ell} \left(\frac{\sigma_\ell}{C_\ell} \right)^{\frac{2\ell+1}{2}} \exp\left(-\frac{2\ell+1}{2} \frac{\sigma_\ell}{C_\ell}\right). \quad (32)$$

We can therefore compute the posterior probability of a set of $\{C_\ell\}$ from M samples $\{\sigma_\ell^i\}$ by

$$\text{Pr}(\{C_\ell\} | \mathbf{d}) \approx \frac{1}{M} \sum_i \text{Pr}(\{C_\ell\} | \{\sigma_\ell^i\}). \quad (33)$$

It is also possible to construct the marginal distributions for any C_ℓ or subset of $\{C_\ell\}$. For a single C_ℓ the marginal distribution can be approximated by

$$\Pr(C_\ell|\mathbf{d}) \approx \frac{1}{M} \sum_i \Pr(C_\ell|\sigma_\ell^i), \quad (34)$$

where

$$\Pr(C_\ell|\sigma_\ell) = \frac{1}{\sigma_\ell} \left(\frac{\sigma_\ell}{C_\ell}\right)^{\frac{2\ell+1}{2}} \exp\left(-\frac{2\ell+1}{2} \frac{\sigma_\ell}{C_\ell}\right). \quad (35)$$

Extremely large numbers of samples would be needed to make this estimator accurate at high ℓ . However even with a relatively small number of samples it forms a useful tool for the analysis of large angular scales. It is worth noting that the expression (33), or its one-dimensional marginalized version (34), do not depend on the $\{C_\ell\}$ -samples, but only on the realization power spectra $\{\sigma_\ell\}$ of the \mathbf{a} -samples.

5 ANALYSIS OF LOW-RESOLUTION SIMULATIONS

To compare the Hamiltonian and Gibbs samplers we applied them both to a set of low-resolution simulations. We produced a map of the CMB with a HEALPix¹ $N_{\text{side}} = 32$ (12288 pixels). Our CMB simulation is a realization of a Λ CDM cosmology with the best fitting parameters from the 5-year WMAP observations² (Spergel et al. 2007) and includes multipoles up to $\ell = 64$. We smoothed the map with a 3-degree Gaussian beam and added isotropic noise with an RMS amplitude of $55\mu K$ per pixel. We chose the noise level so that we could explore how the sampler behaved as a function of the signal-to-noise ratio. We degraded the WMAP Kp2 mask such that any (large) pixel in our final mask is excluded if any of the (small) subpixels in the original mask are excluded. This has the effect of enlarging the Kp2 mask to remove around 30 percent of the sky: a large contiguous area along the Galactic plane and a number of small regions around the locations of bright point sources.

For each sampler we take 20000 burn in samples and then record the next 50000 samples. A large number of samples helps to estimate correlation lengths accurately; far fewer samples are required to explore the distribution. The marginal distributions of a selection of the C_ℓ are shown in Fig. 1. For most ℓ the data is too noisy to constrain the value of the C_ℓ however we do see good agreement between the results from the Gibbs and Hamiltonian samplers. The HMC samples have also been used in conjunction with the Blackwell-Rao estimator to generate a smooth approximation to the marginal distributions. This estimator appears to agree well with the histograms across this range of ℓ , but more samples are likely to be needed if we were to calculate the joint distribution of the $\{C_\ell\}$.

In order to characterise the performance and efficiency of the samplers we considered the correlation of the $\{C_\ell\}$ samples. Assuming that the C_ℓ s are independent we can examine the auto-correlation function,

$$C(n) = \left\langle \frac{C_\ell^i - \langle C_\ell \rangle}{\sqrt{\text{Var}(C_\ell)}} \frac{C_\ell^{i+n} - \langle C_\ell \rangle}{\sqrt{\text{Var}(C_\ell)}} \right\rangle. \quad (36)$$

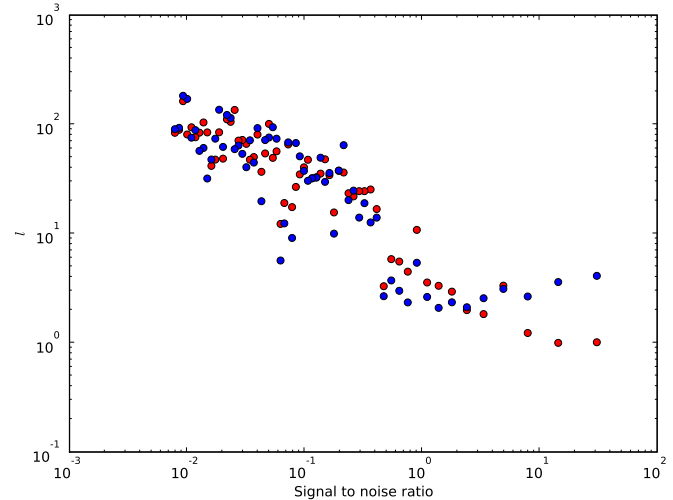


Figure 3. The correlation length (37) as a function of the signal-to-noise ratio of each C_ℓ parameter. The red points show the results from the Gibbs sampler the blue points those from the Hamiltonian sampler.

We show the auto-correlation function for a selection of multipoles in Fig. 2. As the signal-to-noise ratio for a single ℓ , defined as the ratio of the signal and noise power spectra at that ℓ , decreases with increasing ℓ the samples become more highly correlated; it takes more steps of the samplers to generate independent samples. This feature is a well known limitation of the Gibbs sampler caused by the fact that drawing the power spectrum from the conditional distribution $\Pr(\{C_\ell\}|\mathbf{d}, \mathbf{a})$ is limited to the size of the cosmic variance while the joint distribution may be much wider. Similar behaviour is observed with the Hamiltonian sampler although the cause is now related to the difficulty in sampling the highly skewed distributions that occur when the signal-to-noise ratio is low. The correlation length for each parameter can be estimated using

$$l = 1 + 2 \sum_{n=1}^{n_{\text{max}}} C(n), \quad (37)$$

where we truncate the summation at some maximum lag n_{max} at which the auto-correlation function becomes noisy. Fig. 3 shows how the measured correlation lengths for the power spectrum parameters from the Gibbs and Hamiltonian samplers depend on the signal-to-noise ratio for each parameter, again estimated assuming the parameters are independent. We see that in the high signal-to-noise regime the Gibbs sampler performs exceptionally well whereas the Hamiltonian sampler produces samples with typical correlation lengths of around four steps. Once the data becomes noise dominated the picture is less clear with the Hamiltonian sampler generally performing marginally better than the Gibbs sampler. As the signal-to-noise ratio drops below 0.01 both samplers perform poorly.

It is worth noting that Hamiltonian sampler requires around an order of magnitude fewer spherical harmonic transforms (the computationally intensive step in the process) per sample than a Gibbs sampler that uses no preconditioner and around a factor of 3-4 fewer transforms than is reported for Gibbs samplers with carefully tuned preconditioners (Eriksen et al. 2004). Furthermore we have found that the correlation lengths of the Hamiltonian sampler strongly depend on the masses one uses, offering the opportunity for significant improvements given a more sophisticated prescription for setting the masses.

¹ <http://healpix.jpl.nasa.gov>

² <http://lambda.gsfc.nasa.gov/product/map/dr3/parameters.cfm>

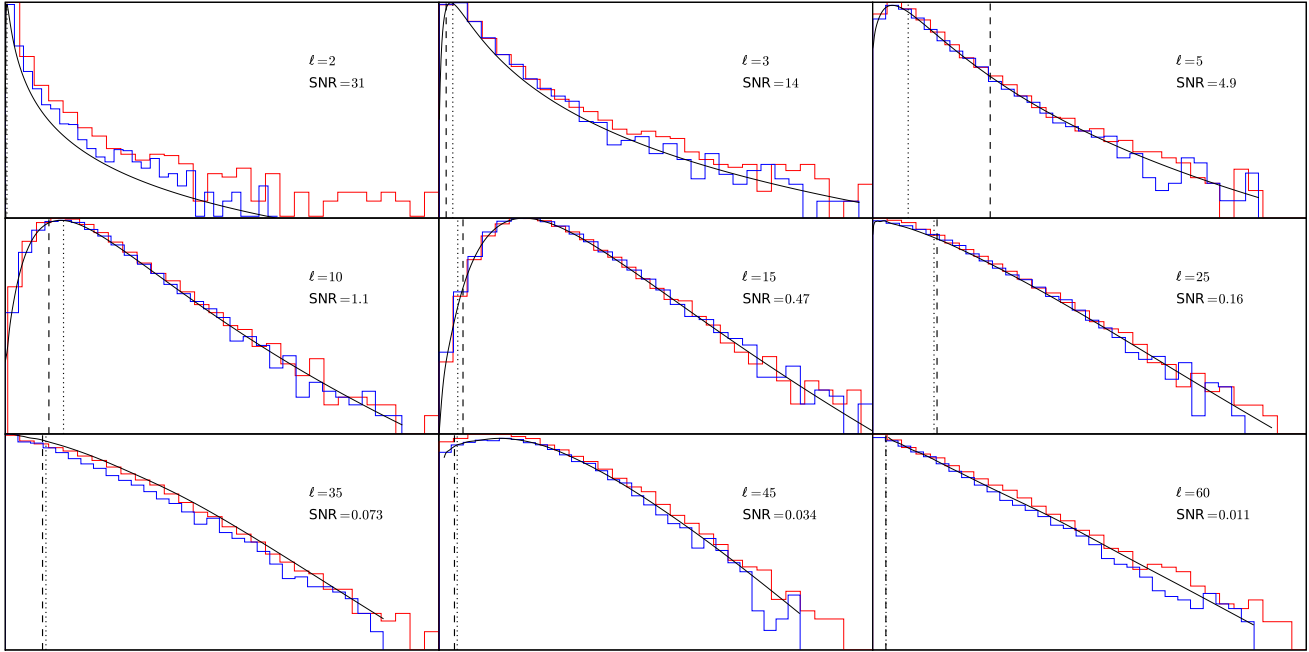


Figure 1. Marginal distributions of C_ℓ samples for a selection of ℓ as shown in the top right corner of each plot along with the signal to noise ratio for this multipole. The results for the Gibbs sampler are shown in red and the Hamiltonian sampler in blue. The plots show the logarithm of the number of samples falling in each bin. The dashed vertical line shows the theoretical value of the C_ℓ used in creating the simulation whereas the dotted vertical line shows the value for the realization. The marginal distributions from the Blackwell-Rao estimator applied to the HMC samples are shown by the smooth black line.

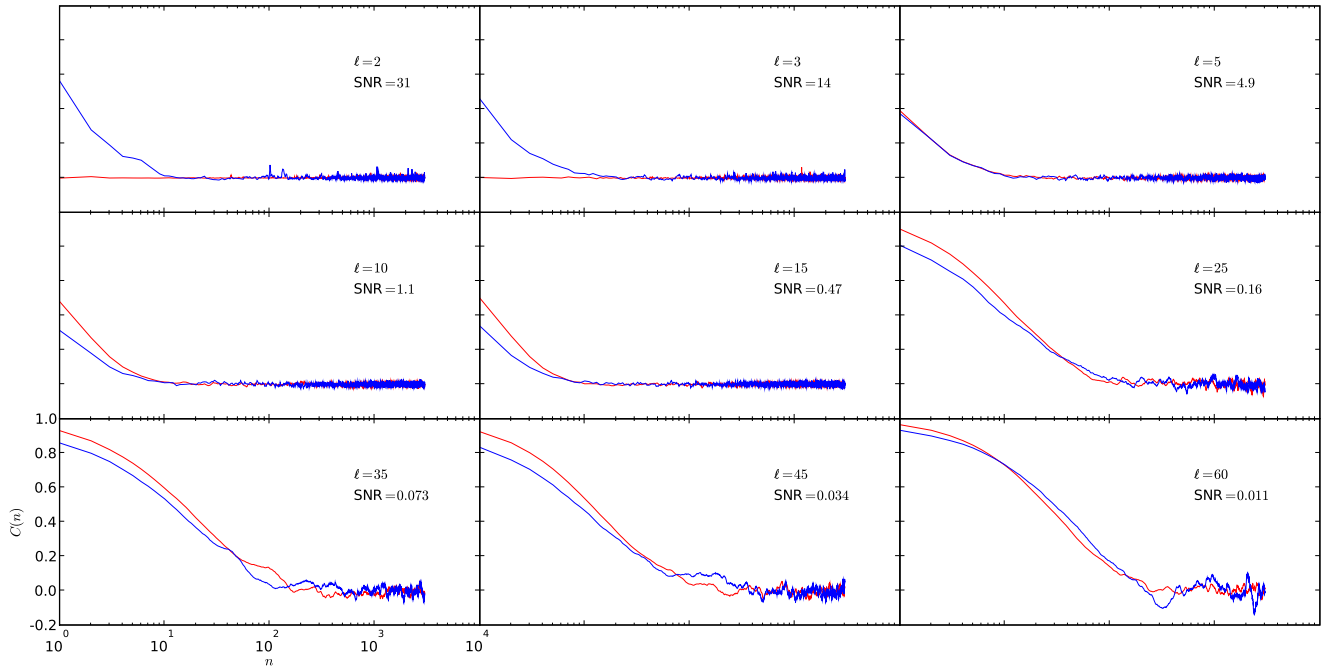


Figure 2. The auto-correlation functions (36) of C_ℓ samples for a selection of ℓ as shown in the top right corner of each plot along with the signal to noise ratio at this multipole. The results for the Gibbs sampler are plotted in red and Hamiltonian sampler in blue. All the plots use the same scale as shown in the bottom left plot.

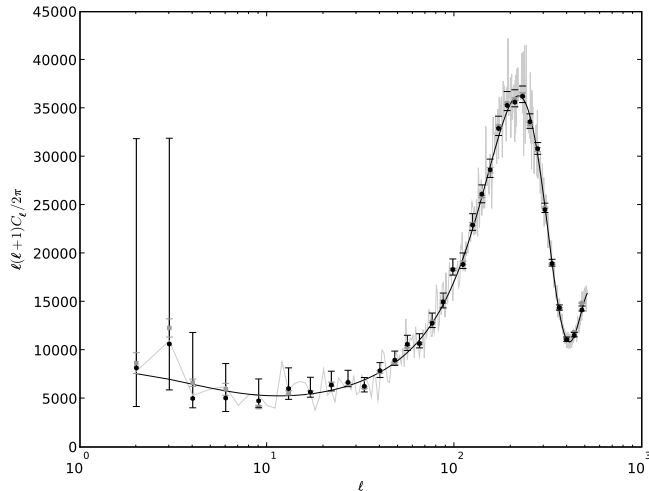


Figure 4. Binned power spectrum and 68 percent confidence intervals as compared to the results of an application of the MASTER method to the same simulated *WMAP* data. The black solid line shows the power spectrum from which the simulation was generated while the grey shows the power spectrum of the realization. The grey squares and error bars show the MASTER results. The black circles and error bars show the peak and 68 per cent confidence intervals found from samples generated with the HMC sampler.

6 ANALYSIS OF SIMULATED *WMAP* DATA

We produce a CMB simulation as for Section 5 but with $N_{\text{side}} = 512$ ($\sim 3 \times 10^6$ pixels) and including multipoles up to $\ell = 512$. The map was then smoothed with a 13-arcmin Gaussian beam, which is similar in size to the beam of the *WMAP* *W*-band. We then added anisotropic uncorrelated noise by making use of the published³ N_{obs} and noise variance for the 5-year *WMAP* combined *W* band map. The map was cut with the Kp2 mask which excludes 15.3% of the sky. We included multipoles up to $\ell_{\text{max}} = 512$ in our analysis. This gives us a total of around 2×10^5 parameters in our sampling space.

To generate a good signal starting point, using a single Gibbs sample, required ~ 800 iterations (20 minutes on the hardware described below) of the conjugate gradient to solve (26) and (27) such that the rms residual was less than 10^{-6} .

For these simulations we made a total of 5000 burn in samples and recorded 10000 samples from the post burn-in phase. It takes ~ 20 seconds to generate a single sample using two dual core Intel Xeon 5150 processors and the MPI parallelised HEALPix spherical harmonic transforms, resulting in a total processing time of around 80 hours.

For comparison we applied the MASTER method (Hivon et al. 2002) to the same data set. Our peak likelihood C_ℓ sample and 68 per cent confidence intervals, binned with the *WMAP* team’s scheme, are shown alongside the results of the MASTER method in Fig. 4. For most of the range of angular scales the two estimates and their errors agree well. On the largest angular scales the MASTER estimate tends to underestimate the uncertainties and the symmetric errors are far from representative of the posterior. In Fig. 5 we show a summary of the convergence statistics, using Hanson’s diagnostic, see Section 3.1, demonstrating that we have fully explored the distribution across the entire

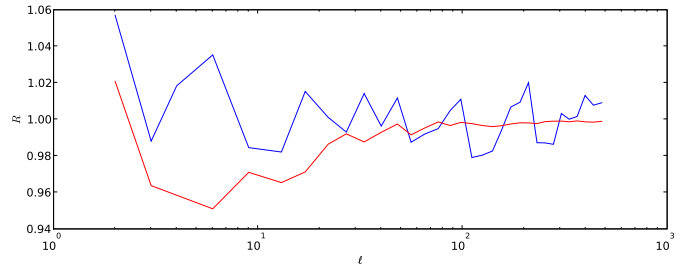


Figure 5. A summary of the convergence statistics of the 10000 samples used to produce the power spectrum in Fig. 4. Although convergence is judged from the R for every parameter we show here only the average R for in each bin for the C_ℓ (blue line) and α (red line). R .

range in ℓ . For all multipoles the R value is within the range 0.9 to 1.1.

7 CONCLUSIONS

We have introduced the HMC sampler for CMB power spectrum estimation and demonstrated its performance both on low-resolution simulations and simulations of 5-year *WMAP* data. We find that the Hamiltonian sampler has similar or shorter correlation lengths when compared to the Gibbs sampler except in the regions of the highest signal-to-noise. Bearing in mind the reduced computational cost and greater flexibility of the Hamiltonian sampler we believe it is an attractive method for performing the analysis.

For high-resolution data sets of size ($N_{\text{side}} = 512$, $\ell_{\text{max}} = 512$) we can generate a sample in ~ 20 seconds on a high-end desktop. This is a significant gain over the reported performance of Gibbs samplers.

HMC requires that we are able to compute the logarithm of the target density and its gradients. Even if exact gradients are not available we can generate approximate trajectories and these will still result in samples drawn from the required distribution. The generality of the approach removes the requirement for strictly Gaussian signal and noise and therefore promises to be an interesting method for tackling a wide range of related problems.

We are currently testing the performance of the method on high-resolution *Planck* simulations and working on extending the method to include polarization. We also intend to apply the technique to the *WMAP* data.

8 ACKNOWLEDGEMENTS

We thank Morgan French for his contributions to the early development of our sampler. JFT acknowledges a STFC (formerly PPARC) studentship. MAJA is a member of the Cambridge Planck Analysis Centre, supported by STFC grant ST/F005245/1. This work was conducted in cooperation with SGI/Intel utilising the Altix 3700 supercomputer at DAMTP Cambridge supported by HEFCE and STFC. We acknowledge the use of the Legacy Archive for Microwave Background Data Analysis (LAMBDA). Support for LAMBDA is provided by the NASA Office of Space Science. Some of the results in this paper have been derived using the HEALPix (Górski et al. 2005) package.

³ <http://lambda.gsfc.nasa.gov>

APPENDIX A: MASSES FOR HAMILTONIAN MONTE CARLO

Hamiltonian Monte Carlo can be extremely sensitive to the choice of masses. When sampling from an approximately isotropic distribution this does not affect the performance significantly but when the marginal distributions of different parameters show considerable variation in width the masses must be set correctly to sample efficiently.

Hanson (2001) suggests that one should set the mass associated with each parameter to be approximately equal to the variance of that parameter in the target density. This is an attempt to circularise the trajectories in the $\{x, p\}$ space. We take an alternative approach, where the mass for a parameter is inversely proportional to the width of the distribution, as suggested in Neal (1996). In order to justify this approach we have generalised the framework in Neal (1993) to describe the application of the leapfrog method.

Consider the problem of sampling from an n -dimensional Gaussian distribution in \mathbf{x} with covariance matrix \mathbf{C} . Our Hamiltonian is quadratic in \mathbf{x} and \mathbf{p}

$$H = \frac{\mathbf{p}^T \mathbf{M}^{-1} \mathbf{p}}{2} + \frac{\mathbf{x}^T \mathbf{C}^{-1} \mathbf{x}}{2}, \quad (\text{A1})$$

where \mathbf{M} is a $n \times n$ mass matrix, and the trajectory will be determined by Hamilton's equations

$$\frac{d\mathbf{x}}{dt} = \nabla_{\mathbf{p}} H = \mathbf{M}^{-1} \mathbf{p} \quad (\text{A2})$$

$$\frac{d\mathbf{p}}{dt} = -\nabla_{\mathbf{x}} H = -\mathbf{C}^{-1} \mathbf{x}. \quad (\text{A3})$$

We integrate the equation of motion with the leapfrog method

$$\mathbf{p}(t + \epsilon/2) = \mathbf{p}(t) - \frac{\epsilon}{2} \mathbf{C}^{-1} \mathbf{x}(t) \quad (\text{A4})$$

$$\mathbf{x}(t + \epsilon) = \mathbf{x}(t) + \epsilon \mathbf{M}^{-1} \mathbf{p}(t + \epsilon/2) \quad (\text{A5})$$

$$\mathbf{p}(t + \epsilon) = \mathbf{p}(t + \epsilon/2) - \frac{\epsilon}{2} \mathbf{C}^{-1} \mathbf{x}(t + \epsilon). \quad (\text{A6})$$

A single application of the leapfrog method can be written in the form

$$\mathbf{x}(t + \epsilon) = \left(\mathbf{I} - \frac{\epsilon^2}{2} \mathbf{M}^{-1} \mathbf{C}^{-1} \right) \mathbf{x}(t) + \epsilon \mathbf{M}^{-1} \mathbf{p}(t) \quad (\text{A7})$$

$$\begin{aligned} \mathbf{p}(t + \epsilon) = & -\epsilon \mathbf{C}^{-1} \left(\mathbf{I} - \frac{\epsilon^2}{4} \mathbf{M}^{-1} \mathbf{C}^{-1} \right) \mathbf{x}(t) + \\ & + \left(\mathbf{I} - \frac{\epsilon^2}{2} \mathbf{C}^{-1} \mathbf{M}^{-1} \right) \mathbf{p}(t), \end{aligned} \quad (\text{A8})$$

where \mathbf{I} is the identity matrix. We can rewrite this in a matrix form

$$\begin{bmatrix} \mathbf{x}(t + \epsilon) \\ \mathbf{p}(t + \epsilon) \end{bmatrix} = \mathbf{T} \begin{bmatrix} \mathbf{x}(t) \\ \mathbf{p}(t) \end{bmatrix}, \quad (\text{A9})$$

where

$$\mathbf{T} = \begin{bmatrix} \left(\mathbf{I} - \frac{\epsilon^2}{2} \mathbf{M}^{-1} \mathbf{C}^{-1} \right) & \epsilon \mathbf{M}^{-1} \\ -\epsilon \mathbf{C}^{-1} \left(\mathbf{I} - \frac{\epsilon^2}{4} \mathbf{M}^{-1} \mathbf{C}^{-1} \right) & \left(\mathbf{I} - \frac{\epsilon^2}{2} \mathbf{C}^{-1} \mathbf{M}^{-1} \right) \end{bmatrix}. \quad (\text{A10})$$

If the method is to be stable under the repeated application of \mathbf{T} then we require its eigenvalues to have unit modulus. The eigenvalues λ are found from the characteristic equation

$$\det \left[\mathbf{I} \lambda^2 - 2\lambda \left(\mathbf{I} - \frac{\epsilon^2}{2} \mathbf{M}^{-1} \mathbf{C}^{-1} \right) + \mathbf{I} \right] = 0. \quad (\text{A11})$$

To explore the space rapidly we wish to find the largest ϵ compatible with the condition for stability. Any dependence of (A11) on \mathbf{C} implies no single value for ϵ will meet the requirement for every eigenvalue to have unit modulus (unless both \mathbf{C} and \mathbf{M} are proportional to the identity matrix). The maximum value for ϵ should therefore be controlled by the width of the distribution for a small subset of parameters.

By setting $\mathbf{M} = \mathbf{C}^{-1}$ we remove the dependence of ϵ on the size of the distribution. In this situation the characteristic equation reduces to

$$\left[\lambda^2 - 2\lambda \left(1 - \frac{\epsilon^2}{2} \right) + 1 \right]^n = 0 \quad (\text{A12})$$

and the stability criterion is met by $\epsilon \leq 2$.

If the dimensionality of the problem is such that it is impractical to perform the required matrix inversion and decomposition of \mathbf{M} (to compute the Hamiltonian and to draw new values for the momentum variables respectively) then simple approximations must be employed. Typically one might construct a diagonal mass matrix with the mass associated with each parameter inversely proportional to the variance of that parameter.

If the distribution to be sampled from is not Gaussian it seems reasonable to use some appropriate measure of the width of the distribution (i.e. the curvature at the peak (Neal 1996)) to set the masses.

REFERENCES

- Bennett C. L. et al., 2003, ApJS, 148, 1
 Bond J., Jaffe A. H., Knox L., 1998, Physical Review D, 57, 2117
 Brooks S., Roberts G., , 1997, Assessing Convergence of Markov Chain Monte Carlo Algorithms
 Challinor A. D., Mortlock D. J., van Leeuwen F., Lasenby A. N., Hobson M. P., Ashdown M. A. J., Efstathiou G. P., 2002, MNRAS, 331, 994
 Chu M., Eriksen H. K., Knox L., Górski K. M., Jewell J. B., Larson D. L., O'Dwyer I. J., Wandelt B. D., 2005, Physical Review D, 71, 103002
 Cowles M. K., Carlin B. P., 1996, Journal of the American Statistical Association, 91, 883
 Duane S., Kennedy A., Pendleton B. J., Roweth D., 1987, Physics Letters B, 195, 216
 Dunkley J., Bucher M., Ferreira P. G., Moodley K., Skordis C., 2005 MNRAS, 356, 925
 Efstathiou G., 2003, MNRAS, 346, L26
 Efstathiou G., 2004, MNRAS, 349, 603
 Eriksen H. K. et al., 2004, ApJS, 155, 227
 Gelman A., Rubin D. B., 1992, Statistical Science, 7, 457
 Golub G. H., Loan C. F. V., 1996, Matrix Computations. The John Hopkins University Press
 Gorski K. M., 1994, ApJ, 430, L85
 Górski K. M., Hivon E., Banday A. J., Wandelt B. D., Hansen F. K., Reinecke M., Bartelmann M., 2005, ApJ, 622, 759
 Hajian A., 2007 Physical Review D, 75, 083525
 Hanson K. M., 2001, Proc. SPIE, 4322, 456
 Hivon E., Górski K. M., Netterfield C. B., Crill B. P., Prunet S., Hansen F., 2002, ApJ, 567, 2
 Hobson M. P., Masinger K., 2002, MNRAS, 343, 569
 Jewell J., Levin S., Anderson C., 2004, ApJ, 609, 1
 Neal R., 1993, Technical report, Probabilistic Inference Using

- Markov Chain Monte Carlo Methods. Department of Computer Science, University of Toronto
- Neal R., 1996, Bayesian Learning for Neural Networks. Springer-Verlag New York
- Oh S. P., Spergel D. N., Hinshaw G., 1999, ApJ, 510, 551
- Spergel D. N. et al., 2007, ApJS, 170, 377
- Wandelt B. D., Hansen F. K., 2003, Physical Review D, 67, 023001
- Wandelt B. D., Larson D. L., Laksminarayana A., 2004, Physical Review D, 70, 083511
- Zaldarriaga M., Seljak U., 1997, Physical Review D, 55, 1830